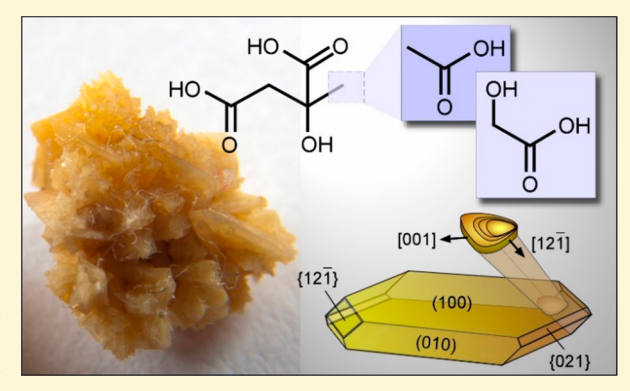


Factors Differentiating the Effectiveness of Polyprotic Acids as Inhibitors of Calcium Oxalate Crystallization in Kidney Stone Disease

Jihae Chung,[†] Michael G. Taylor,[‡] Ignacio Granja,[§] John R. Asplin,[§] Giannis Mpourmpakis,[‡] and Jeffrey D. Rimer*, To

Supporting Information

ABSTRACT: Pathological crystallization of calcium oxalate monohydrate (COM) is a critical process in human kidney stone disease. Methods of curtailing COM growth involve the action of natural and synthetic polyprotic acids, which selectively bind to crystal surfaces and inhibit the anisotropic rates of growth. Here we use a combination of bulk crystallization, in situ scanning probe microscopy, density functional theory, and physiologically relevant in vitro assays to elucidate the molecular origins of COM growth inhibition, focusing on citrate (CA) and its molecular analogues hydroxycitrate (HCA) and isocitrate (ICA). These three molecules differ only in the number and/or placement of hydroxyl groups, yet each exhibit unique binding modes to COM crystal surfaces. A major breakthrough in the development of potential therapies came from the recent discovery of HCA being



a potent inhibitor possessing an ability to dissolve crystal surfaces in supersaturated media. Using a combination of experiments and computational calculations, we examine the differentiating factors for isostructural analogues of citrate to prompt dissolution and introduce a vectorized displacement parameter that accounts for strain induced on a crystal lattice as a result of inhibitor adsorption. We also compare the inhibitory effects of all three polyprotic acids in a human urine assay that surprisingly revealed HCA to be a far superior inhibitor than laboratory estimates owing to an apparent synergistic cooperative effect with species in the urine milieu. Collectively, these findings identify new inhibitors of calcium oxalate crystallization and demonstrate that HCA and ICA are promising alternatives to citrate, the current therapy.

■ INTRODUCTION

Crystallization is a ubiquitous phenomenon in biological systems and is also common to several diseases that include malaria, gout, atherosclerosis, gallstones, and urolithiasis (or kidney stones). Prevention of these diseases often involves the use of natural or synthetic molecules (or macromolecules) that act as inhibitors of crystal growth. These species exhibit a specificity for binding to particular surfaces of pathological crystals and reduce their rate of growth by one of several possible modes of action.^{6,7} There is an extensive volume of literature on inhibitors in biomineralization, particularly those systems involving calcium minerals. $^{8-10}$ Examples of calcification in biology include the formation of shells in mollusks, 9,11,12 structural motifs in coccoliths, 13 and the inorganic matrix of bone. 14 The vast majority of inhibitors in these processes tend to be polyprotic acids comprised of carbonates and/or phosphates that interact with crystals via the formation of ionic bonds with calcium. Inhibitors can either operate as expedient regulators of crystallization (e.g., generation of skeletal structures), or they can serve as a natural defense against the formation of crystals

with detrimental outcomes (e.g., pathological diseases). The objective of this study is to identify polyprotic acids that inhibit the growth of calcium oxalate monohydrate (COM), a principal component of human kidney stones. $^{15-17}$

Kidney stone disease affects nearly 10% of the population, and while recent reports indicate that incidence rates are on the rise, 18 there has been no significant advancement in the past 30 years to develop therapeutics that more effectively inhibit COM crystallization. Prior studies have shown that inhibitors decorated with carboxylic acids are operative modifiers of COM crystallization. Acid groups interact with crystal surfaces via calcium bridges, (inhibitor)COO-···Ca²⁺···-OOC(COM), or hydrogen bonds, -COO-...HOOC-. Several native proteins in urine that function as putative inhibitors of calcium oxalate stones are rich in acidic amino acids, such as glutamic (Glu) and aspartic (Asp) acids. $^{19-23}$ Examples include (but are not limited

Received: June 20, 2018 Revised: July 25, 2018 Published: July 27, 2018

Department of Chemical and Biomolecular Engineering, University of Houston, Houston, Texas 77204, United States

[‡]Department of Chemical Engineering, University of Pittsburgh, Pittsburgh, Pennsylvania 15261, United States

[§]Litholink Corporation, Laboratory Corporation of America Holdings, Chicago, Illinois 60612, United States

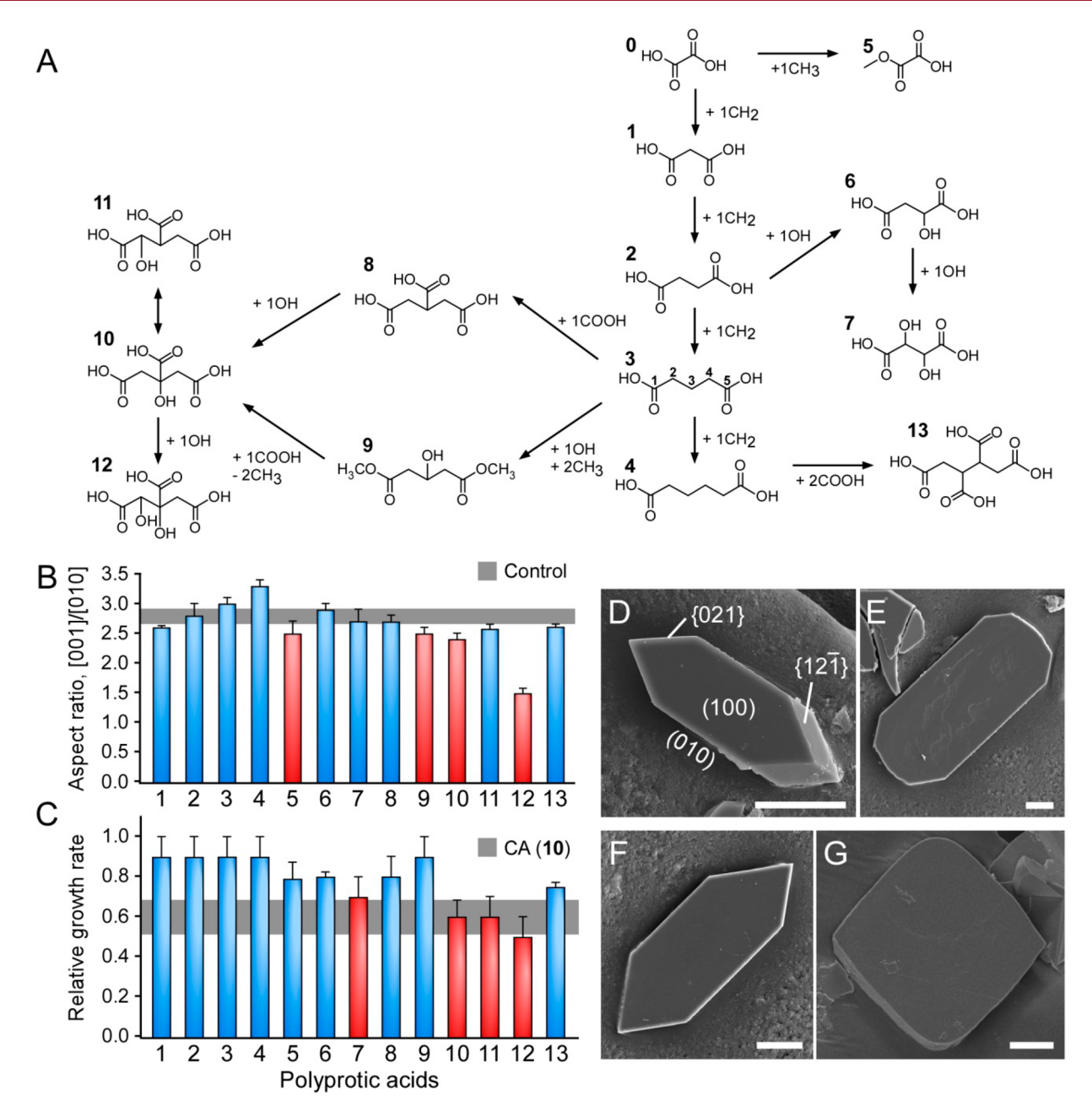


Figure 1. Molecular structures of polyprotic acids and their effect on COM crystallization. (A) The homologous series of putative growth inhibitors selected for this study are numbered as follows: (0) oxalic acid, Ox; (1) malonic acid, MA; (2) succinic acid, SA; (3) glutaric acid, GA; (4) adipic acid, AA; (5) methyl oxalic acid, MOA; (6) malic acid, MCA; (7) tartaric acid, TTA; (8) tricarballylic acid, TCA; (9) dimethyl hydroxyglutaric acid, DHGA; (10) citric acid, CA; (11) isocitric acid, ICA; (12) hydroxycitric acid, HCA; and (13) butanetetracarboxylic acid, BTCA. (B) Aspect ratio of COM crystals (i.e., c/b dimensions) prepared in the absence (control) and in the presence of polyprotic acids. The gray bar signifies two standard deviations for the control. Average values were calculated from at least three separate batches. (C) Relative growth rate (RGR) determined by comparing the COM crystallization rate in the presence of $60 \mu g/mL$ inhibitor to the control. The gray box denotes two standard deviations for the benchmark, CA. Data are the average of at least six independent measurements. (D–G) Scanning electron micrographs of COM crystals in the absence (D) and in the presence of citrate (E), isocitrate (F), and hydroxycitrate (G) using a fixed concentration of $60 \mu g/mL$ inhibitor. Error bars equal one standard deviation; scale bars equal $20 \mu m$.

to) osteopontin, Tamm Horsfall protein, serum albumin, transferrin, bikunin, and prothrombin fragment 1.^{21,24–26} The addition of acid groups to a molecule generally results in increased efficacy. For instance, amino acids (e.g., Glu and Asp) inhibit the rate of COM crystal growth by ca. 35%, whereas polyamino acids comprised of the same monomers exhibit ca. 85% inhibition.²⁷ The current therapy administered to calcium oxalate kidney stone patients is citrate (CA), a molecule with

three carboxylic acids available to interact with COM crystals. *In vitro* bulk crystallization assays reveal that CA imparts a maximum 60% inhibition of COM crystallization. Recently, it was discovered that hydroxycitrate (HCA), a structural analogue of CA with one additional alcohol moiety, is more potent than CA. Recently,

Understanding the factors that govern inhibitor specificity and efficacy is nontrivial. Small organic acids, such as CA and

HCA, are generally less effective crystal growth inhibitors than the majority of polyprotic macromolecules, yet the former can impart unique effects on COM crystallization that, in many respects, make them more desirable crystal growth inhibitors. For instance, it was recently shown that HCA and to a lesser extent CA are capable of dissolving COM crystals in supersaturated media. This phenomenon was observed by in situ atomic force microscopy (AFM) under continuous flow of growth solution wherein COM dissolution occurs within a narrow range of inhibitor concentration.²⁸ The proposed mechanism involves the generation of strain at the crystal surface imposed by inhibitor adsorption. In the case of HCAcrystal interactions on the COM (121) surface, density functional theory (DFT) calculations indicated a displacement of atoms within the crystal lattice where it was hypothesized that the resulting strain was relieved by the dissolution of calcium and oxalate from the crystal interface. At concentrations below the critical range for dissolution, COM growth rates are reduced in the presence of inhibitor, similar to classical models of crystal growth inhibition. The mechanism at high inhibitor concentration is more nuanced in that a high coverage of inhibitor has two potential effects: (i) mass transport limitations owing to the steric constraints of inhibitor adsorption/desorption coupled with the release of solute from the interface, and (ii) the generation of roughened interfaces with a higher density of kink sites, which are the most energetically favorable for solute incorporation, thus leading to an enhanced rate of crystal growth. More recently, the mechanism of strain-induced dissolution was demonstrated by Li et al.²⁹ for brushite (CaHPO₄·2H₂O), another kidney stone constituent, in the presence of HCA in which the dissolution was attributed to the localized strain in crystal lattice due to strong HCA-brushite interactions.

Here, we examine a library of polyprotic acids to identify a broader class of COM growth inhibitors and refine the criterion for strain-induced dissolution. Counter to conventional wisdom, our findings reveal that the vast majority of polycarboxylate molecules are ineffective inhibitors of COM crystal growth. Moreover, we show that inhibitor-crystal binding energy is an insufficient descriptor for predicting dissolution. Through the systematic screening of polyprotic acids, we identify a possible replacement for CA as a therapy and show that HCA is a substantially more effective inhibitor of COM crystallization in urine compared to the biomimetic growth solutions employed in previous studies. The latter finding suggests that HCA works cooperatively with other biomolecules in physiological environments to enact greater inhibitory effects on COM formation. It also highlights the disparate behavior of some modifiers assessed in human urine compared to model (more simplistic) growth media employed in vitro.

RESULTS AND DISCUSSION

Homologous Series of Polyprotic Acids. In search of potential inhibitors of COM crystal growth, we examined a series of polyprotic acids in Figure 1A, which are differentiated on the basis of their molecular size and number/type of functional moieties. The library consists of di-, tri-, and tetracarboxylic acids. The simplest dicarboxylic acid is oxalate (Ox, 0), a principal component of COM crystals. We examined the effect of several dicarboxylic acids with varying carbon chain length: malonic acid (MA, 1), succinic acid (SA, 2), glutaric acid (GA, 3), and adipic acid (AA, 4). Molecules with additional carboxylic acid groups include tricarballylic acid (TCA, 8) and

butanetetracarboxylic acid (BTCA, 13). The addition of alcohol groups increased the pool of candidates to six additional molecules (6, 7, 9–12) as a means of examining the impact of alcohol number and their spatial positioning along the carbon backbone. Moreover, we examined the substitution of a carboxylic acid of oxalate with a methyl ester (MOA, 5). Collectively, the library of polyprotic acids in Figure 1A represents a homologous series of putative inhibitors that were used to assess the relationship between inhibitor structure and performance (i.e., inhibitor efficacy and specificity) in COM crystal growth.

One of the metrics for assessing inhibitor specificity for binding to particular COM (hkl) surfaces is the change in length-to-width aspect ratio of COM crystals in bulk crystallization assays. The aspect ratio is measured along the crystallographic [001] and [010] directions, respectively. Growth solutions in the absence of inhibitor (control) yield an aspect ratio of 2.8 ± 0.1 (gray box in Figure 1B and Figure S1). Inhibitors that increase the aspect ratio relative to the control indicate a preferential binding to COM {010} surfaces, whereas a decreased aspect ratio indicates a preferential binding to either the $\{001\}$ surfaces or the apical $\{12\overline{1}\}$ and/or $\{021\}$ surfaces. Molecules 2−4 yield a progressive increase (≤20%) in aspect ratio with increasing chain length. Five molecules reduce COM crystal aspect ratio in the follow order (from highest to lowest): $11 \approx 13 > 9 > 10 > 12$. Parallel kinetic studies of COM crystallization were performed using an ion-selective electrode 24,28,30-32 to track the temporal depletion of free calcium ions. Here we report the relative growth rate (RGR), which is the ratio of COM crystal growth rate in the presence of inhibitor to that of the control, where RGR < 1 indicates COM growth inhibition. As a benchmark, we use citrate (Figure 1C, gray box), the current therapy for COM kidney stones. The RGR of citrate (CA) is 0.6, indicating a 40% reduction in the rate of COM crystallization. Molecules with comparable or better inhibitory effect on COM crystallization are highlighted in red (7, 11, and 12). We have previously shown that hydroxycitrate (HCA) is an effective inhibitor of COM growth.²⁸ Our findings here reveal that isocitrate (ICA) and CA are comparable inhibitors, whereas tartaric acid (TTA) is moderately effective. All remaining molecules that were tested had only a marginal impact on COM crystallization (i.e., RGR \geq 0.8).

RGR comparisons reveal that the addition of carboxylic acids generally increases inhibitor efficacy, but not to the extent that would be expected based on prior studies of polyelectrolytes.³² For example, macromolecules such as polyglutamic acid decorated with many carboxylic acids exhibit RGR values as low as 0.2 compared to their respective amino acids (e.g., glutamic acid) which have values of ca. 0.65. 32 Here we observe only a slight reduction in RGR between glutaric acid (0.9 ± 0.1) and tricarballylic acid (0.8 ± 0.1) with the insertion of one acid group. There is a more noticeable difference between the RGR of adipic acid (0.9 ± 0.1) and butanetetracarboxylic acid $(0.75 \pm$ 0.02) via the addition of two acid groups; however, the performance of these molecules is less than that of the benchmark (citrate) and acidic amino acids. Interestingly, the addition of alcohol groups has a more pronounced effect. For instance, the comparison of molecules with a similar carbon chain length reveals a progressive decrease in RGR with alcohol addition: succinic acid (0.9 \pm 0.1, 0 OH) > malic acid (0.80 \pm 0.02, 1 OH) > tartaric acid (0.7 \pm 0.1, 2 OH). Likewise, we observe a decrease in RGR for citrate analogues with an increasing number of alcohol groups: tartaric acid (0.8 \pm 0.1, 0

OH) > citrate $(0.60 \pm 0.08, 1 \text{ OH}) \approx \text{isocitrate } (0.6 \pm 0.1, 1 \text{ OH}) > \text{hydroxycitrate } (0.5 \pm 0.1, 2 \text{ OH}).$

One molecule that was less effective than anticipated was methyl oxalic acid (MOA, 5). The selection of MOA was motivated by previous studies of L-cystine 33 kidney stones where it was reported that chemical modification(s) to the solute, such as the replacement of carboxylic acids with methyl esters, generated "tailored" inhibitors. A similar approach applied to Ox by replacing a single carboxylic acid group with an ester resulted in RGR = 0.79 ± 0.08 , which is less effective than CA; however, MOA does alter the aspect ratio (Figure 1B), indicating an interaction with crystal surfaces, but not to an extent that these interactions markedly reduce the overall rate of COM crystallization.

Our analysis of polyprotic acids in Figure 1A indicates that not all acids function as COM growth inhibitors and that simply adding more acid groups to a molecule does not necessarily enhance its efficacy; however, we do observe a distinct trend in growth rate suppression based on the magnitude of the second dissociation constant, pK_{a2} , of the acid. This parameter was selected as a potential metric for distinguishing acid group affinity for binding cations (e.g., the interaction between dissociated acids and calcium ions). As shown in Figure 2, the

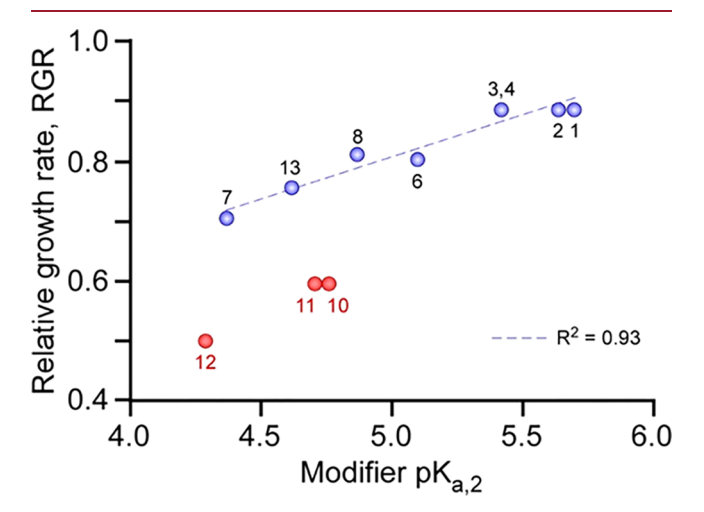


Figure 2. Trends in polyprotic acid inhibition of COM based on their acid strength. The RGR for inhibitors in Figure 1C are replotted here as a function of their respective pK_{a2} values. Listed numbers for each molecule are defined in Figure 1A and pK_{a2} values, and their corresponding references, are provided in Table S1. The dashed line is a linear regression of blue symbols with $R^2 = 0.93$. Red symbols, which correspond to citrate analogues, are outliers.

relative growth rate of COM crystals decreases linearly with decreasing polyprotic acid pK_{a2} . All experiments in this study were conducted at pH 6.2, which is above the pK_{a2} values of all acids tested, indicating that the inhibitors are fully dissociated. Thus, the increased efficacy of inhibitors seems to correlate with the increased acid strength of the polyprotic acid. Exceptions to this trend, however, are the three citrate analogues (red symbols in Figure 2), which indicate that the presence of alcohols enhances the effects of these molecules. Indeed, the most effective COM growth inhibitors among this library are citrate (CA, 10) and its molecular analogues isocitrate (ICA, 11) and hydroxycitrate (HCA, 12), which differ only by the number and/or position of alcohol groups. Scanning electron micrographs of COM crystals reveal distinct differences in the morphology of crystals prepared in the presence of these

inhibitors compared to the control (Figure 1D). Prior studies report 35,36 that CA binds to COM $\{001\}$ surfaces and blunts the apical tips (Figure 1E). HCA binds to both $\{12\overline{1}\}$ and $\{021\}$ surfaces 28 to generate diamond-shaped crystals (Figure 1G). The interaction between ICA and COM crystals preserves the hexagonal morphology (Figure 1F) but results in a reduction in the [100] thickness (Figure S2) with a concomitant decrease in the surface area of apical facets. Thus, electron micrographs indicate that all three inhibitors exhibit unique modes of binding to COM crystals. Herein, we shift our focus to these three inhibitors to examine their effects in greater detail.

Modes of COM Growth Inhibition. We use a combination of atomic force microscopy (AFM) and density functional theory (DFT) to provide a molecular level description of inhibitor-COM interactions for citrate analogues. These studies focus solely on the COM (100) basal surface, which is comprised of steps that are favorable for HCA and CA adsorption and terraces that are preferential binding sites for ICA. In situ AFM measurements of step advancement on the basal surface (Figure 3A) at a fixed inhibitor concentration (0.2 μg/mL) confirmed that all three molecules reduce step advancement in the [001] direction relative to the control. Notably, we observe the following trend in step velocity: HCA < CA < ICA. In a previous study, ²⁸ we showed that both HCA and CA are capable of dissolving COM crystals within a specific range of inhibitor concentration. Here we intentionally selected a concentration that leads to three distinct effects with respect to step velocity ν : CA nearly arrests step advancement ($\nu \approx 0$), HCA dissolves the surface (ν < 0), and ICA reduces the rate of step advancement by ca. 60% (0 < ν < ν_o). Time-resolved AFM images of the COM basal surface show triangular hillocks emanating from a dislocation with steps that advance across the surface in the c-direction. Dissolution of this surface in the presence of HCA (Figure 3B) results in steps receding toward the center of the dislocation. Introduction of HCA leads to a slight roughening of steps, but has little impact on interstep distances. Conversely, the presence of ICA reduces interstep distance relative to the control (Figure 3C,D and Figure S3); however, AFM measurements over a broad range of concentration (e.g., $C_{ICA} = 0.4-40 \mu M$) revealed that ICA does not dissolve COM crystals.

AFM measurements of COM layer growth in the presence of ICA show a monotonic reduction in ν with increased inhibitor concentration (Figure 3E). Comparison of ICA with its isomer CA (reported by Weaver et al.³⁷) reveals a similar trend in step velocity, which is indicative of a step pinning³⁸ mechanism wherein ICA adsorbs on (100) terraces and impedes the advancement of steps across the surface. The velocity profiles were plotted in Bliznakov coordinates,³⁹ which are used to identify modifiers that operate by a kink blocking mode of action. The nonlinear behavior observed in the Bliznakov plot (Figure S4) indicates the mechanism is not kink blocking. This is consistent with bulk crystallization data showing ICA binds to terraces on the basal surface, thereby inhibiting normal growth. Indeed, theoretical models of spiral growth predict the rate of crystal growth normal to the surface of imaging is

$$G_{[100]} = \frac{\nu \cdot h}{y} = \frac{h}{\tau} \tag{1}$$

where $G_{[100]}$ is the rate of crystal growth normal to the basal (100) surface, h is the height of steps advancing along the (100) plane, y is the interstep distance, and τ (= y/v) is the

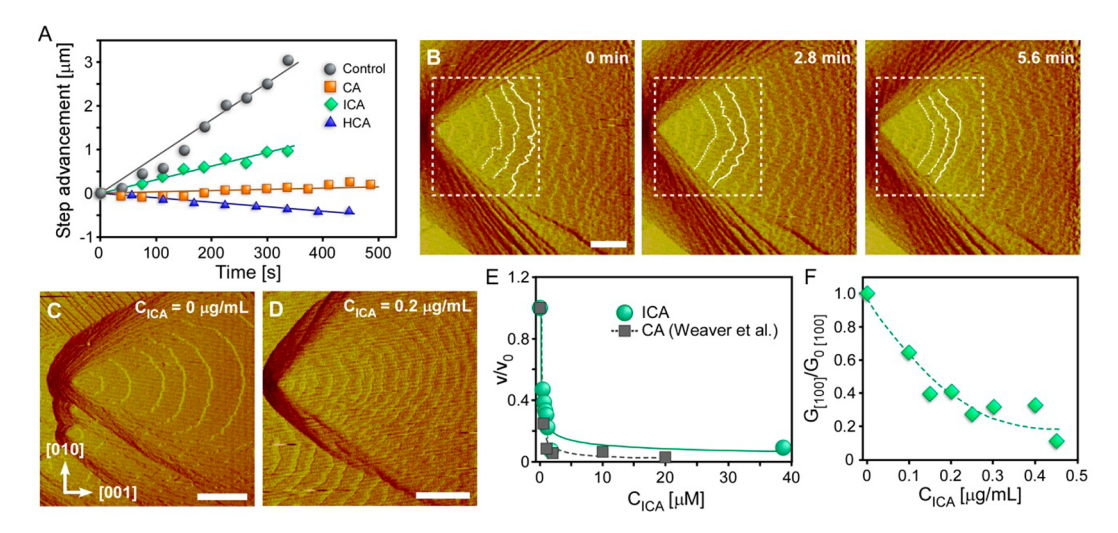


Figure 3. Impact of citrate analogues on COM (100) surface growth. (A) In situ AFM measurements of step advancement in the c-direction as a function of time in the absence of inhibitor (gray circles) and with 0.2 μ g/mL of ICA (green diamonds), CA (orange squares), and HCA (blue triangles). The [001] step velocity, v, was calculated from the slopes of each curve. (B) Snapshots of steps receding in the presence of $C_{HCA} = 0.2 \mu$ g/mL. Select steps are traced with white lines to highlight receding layers during dissolution (the dashed box is placed in a fixed location as a reference). (C and D) Deflection mode images of a surface growing in the absence of inhibitor (C) and in the presence of 0.2μ g/mL ICA (D). (E) Step velocity scaled by the control, v_o , as a function of ICA concentration C_{ICA} . Symbols are the average of at least five measurements and error bars equal two standard deviations. Similar measurements for CA reported by Weaver et al. ³⁷ are plotted as gray squares. (F) Normal rate of growth in the [100] direction calculated using eq 1 and scaled by the control. The dashed line is interpolated to guide the eye. All scale bars in micrographs equal 1 μ m.

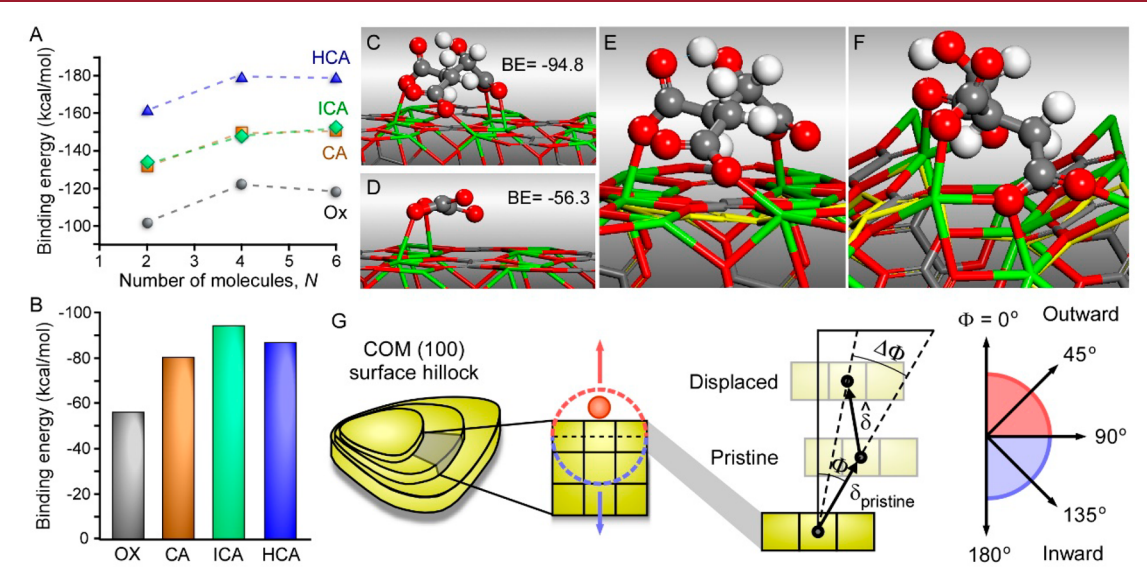


Figure 4. Inhibitor-crystal binding energies. (A) DFT-calculated binding energy of fully dissociated HCA, CA, ICA, and Ox molecules interacting with free calcium ions. Data are plotted against the number of molecules N. Note that D-isocitrate was used for all DFT calculations (refer to Figure S7 for calculations of the enantiomer L-isocitrate). (B) DFT calculations of the binding energy between deprotonated polyprotic acids and the COM (100) surface. (C and D) Structural conformation and binding energy (in kcal/mol) of (C) ICA and (D) Ox adsorption on a frozen COM (100) surface. Atoms are color coded as carbon (gray), hydrogen (white), oxygen (red), and calcium (green). (E and F) Structural conformation of (E) ICA on a COM (100) surface and (F) ICA on a COM (021) surface. Yellow lines represent the relaxed COM crystal lattice upon adsorption of each polyprotic acid relative to the frozen (i.e., idealized) surfaces. (G) Schematic depicting the vectorization of strain $\hat{\delta}$ upon adsorption of inhibitors to COM crystal surfaces. The callout scheme depicts an example of outward displacement (Φ < 90°). Relaxation of the crystal surface in the absence of inhibitors shifts the pristine lattice by an angle Φ and distance $\hat{\delta}_{pristine}$. Strain fields induced by inhibitors pulling atoms in the lattice (calcium and oxalate) outward from the surface (red) or pushing them inward (blue) at a net angle $\Delta\Phi$ (relative to the pristine surface) and displace the crystal plane by $\hat{\delta}$.

characteristic rotation time of layers propagating from the screw dislocation. The average height of the layers is constant (within 20%) over the full range of ICA concentrations; therefore, we approximated $G_{[100]}$ using velocity data in Figure 3E and the corresponding interstep distances in Figure S3. The monotonic reduction in $G_{[100]}$ (Figure 3F) with increasing C_{ICA} is consistent

with bulk crystallization showing that ICA reduces the [100] thickness of COM crystals (Figure S2).

We performed DFT calculations to further understand the modes of inhibitor action. As a starting point, we examined the affinity of solute (Ox) and inhibitors to complex free calcium ions in solution (Figures 4A and S5), comparing ICA to previous results for Ox, CA, and HCA.²⁸ The binding energy (BE)

between each inhibitor and calcium ions was calculated as a function of the number of molecules, wherein each calcium cation interacts with two carboxylic acid groups. Plots of BE in Figure 4A reveal the following order (from strongest to weakest binding, with the negative values denoting exothermic/favorable interaction): $HCA > ICA \approx CA > Ox$. This order qualitatively agrees with the relative growth rates measured in bulk crystallization assays (Figure 1C), and seemingly scales with the acid strength of each molecule (Figure 2). To elucidate inhibitor-COM interactions at a molecular level, we used DFT to calculate the binding of each inhibitor to the COM (100) surface (Figures 4B and S6). The binding energy of ICA to COM (100) is the strongest (Figure 4C), whereas Ox is the weakest (Figure 4D). The preferential binding of ICA to the basal surface agrees with the step pinning mechanism identified by in situ AFM (Figure 3) and the reduced [100] thickness of COM crystals observed in bulk crystallization assays (Figure S2).

In Table 1 we present the DFT calculated BE and structural results on COM (100) and (021) surfaces along with the

Table 1. DFT Calculations a of Binding Energies and Lattice Displacements b

$interaction^c$	$BE_{(021)}/BE_{(100)}^{d}$	$\delta_{(021)}/\delta_{(100)}$	$\Phi_{(100)}\left(\Delta\Phi\right)$	$\Phi_{(021)}\left(\Delta\Phi ight)$
HCA-COM	1.95	2.84	148° (+27°)	46° (-3°)
CA-COM	1.82	2.20	173° (+52°)	$49^{\circ}\ (0^{\circ})$
ICA-COM	1.61	2.04	175° (+53°)	53° (+4°)
pristine COM		2.24	121° (-)	49° (-)

^aDetailed calculations are provided in Table S2 and Figure S8 in the Supporting Information. ^bFor each inhibitor, the value of Φ is given in addition to its value relative to the pristine COM relaxation in parentheses. ^cInteractions of fully dissociated acids. ^dBinding energy calculated in units of kcal/mol.

pristine COM surface (i.e., relaxation in the absence of inhibitor). The relative BE reveals a preferential interaction of inhibitors with the (021) surface in the order: HCA > CA > ICA. This is consistent with bulk crystallization assays and *in situ* AFM studies ²⁸ (Figure 1B) showing that HCA preferentially binds to the $\{021\}$ and $\{12\overline{1}\}$ apical surfaces. *In situ* AFM measurements on the COM (010) surface reveal that CA has no effect on either the $\{021\}$ or $\{12\overline{1}\}$ step velocities. ³⁶ Similar findings in this study reveal that ICA also does not alter step advancement on the (010) surface (Figure S8). Collectively, these findings are consistent with bulk crystallization revealing CA binds to (001) faces while ICA binds to (100) faces, and are consistent with DFT calculations of inhibitor specificity for different COM crystal surfaces (see the SI for more details on DFT calculations of BE).

Binding energy is an effective descriptor for inhibitor-crystal specificity but cannot be used as the sole parameter to rationalize surface dissolution. Previously, Chung et al. introduced the concept of strain-induced dissolution wherein the net displacement δ of atoms in the crystal lattice with inhibitor binding was used as an analogue of strain. Calculation of δ involves the partial relaxation of COM crystal surfaces following inhibitor adsorption to evaluate the impact of these interactions on the surface structure of COM crystals. For illustration, Figure 4E,F shows how the (100) and (021) faces respond during surface relaxation in the presence of adsorbed ICA molecules. Using the difference between the frozen and relaxed COM surfaces, we calculated δ , but here we introduce the calculation of the angle of

surface displacement (Φ) to gain a deeper understanding of surface relaxation and dissolution (Table 1). Comparisons are made using the ratio of δ values on the (021) and (100) surfaces relative to the pristine COM surfaces (i.e., relaxation in the absence of inhibitor). We note that these pristine COM relaxations establish a common reference for displacement with all modifiers. For all cases, the (021) surface exhibits more strain than the (100) surface. This agrees with the observation that certain inhibitors (e.g., HCA) can dissolve (021) steps, while none of the polyprotic acids appear to dissolve (100) faces. Comparisons of CA and HCA reveal the latter more effectively dissolves COM crystals. The relative magnitude of δ values can rationalize the observed dissolution of (021) over (100) surfaces. Comparison of HCA, CA, ICA, and pristine δ ratios (Table 1) shows the trend HCA > pristine \approx CA > ICA, which agrees with experimental observations that HCA can dissolve COM {021} faces, while CA and ICA cannot. It should be noted, however, that we previously reported²⁸ that CA binding to (001) steps on the basal surface can lead to the formation of etch pits at specific conditions not tested in this study.

To reveal further insights into the action of citrate analogues on the surface of COM, we introduce a vectorized strain that accounts for its direction of displacement. The schematic illustrating Φ in Figure 4G indicates that adsorbed inhibitors can induce a strain by "pulling" on the surface, resulting in negative $\Delta\Phi$ relative to pristine surface relaxation. Conversely, the adsorbed inhibitor can "push" on the surface, giving rise to positive $\Delta\Phi$ relative to pristine surface relaxation. Since the negatively charged modifiers interact directly with Ca²⁺ ions at the surface, a negative $\Delta\Phi$ indicates Ca^{2+} ions in the COM surface are being pulled away from the surface, suggesting directionality to COM surface dissolution. DFT calculations of inhibitor binding to the COM (100) surface reveal inward $\Delta\Phi$ angles between +27° and +53°. Additionally, ICA displays a similar behavior on the (021) surface, imposing a +4° relative relaxation angle compared to the pristine calculation. Conversely, measurements of HCA and CA binding to the COM (021) surface reveal that HCA imposes a relative displacement with an outward angle (-3°) , whereas CA does not exhibit any imposed directionality at this interface (i.e., $\Delta \Phi = 0^{\circ}$). It should be noted that the sign of $\Delta\Phi$ is used as a criterion to rationalize the directionality of strain and not its magnitude, which may depend on several parameters, such as the computational details, and the stability of each facet and adsorption site, among others. The combination of a large BE, large δ , and outward $\Delta\Phi$ ($\Delta\Phi$ < 0) is what differentiates HCA from CA and ICA in its ability to dissolve COM crystals. The unique directionality of the strain induced by HCA is likely due to the additional hydrogen bonding present on HCA, favoring more spherical shapes upon adsorption (see Figure S8). As such, we expand our previous criterion for surface dissolution by stating that an inhibitor must preferentially bind a specific facet with high BE and simultaneously induce a displacement with $\Delta\Phi$ < 0° relative to the pristine surface.

Replacing Citrate with Alternative Therapies. The criteria for identifying an alternative therapy for calcium oxalate stone disease relies on the identification of a molecule that has some or all of the following characteristics: (1) better tolerated than CA, (2) sufficiently bioavailable, (3) complexes calcium as well as or better than citrate, and (4) inhibits COM crystallization (preferably more so than citrate). In addition, the metabolism of citrate leads to systemic alkalinization, which may be detrimental in patients with a high urine pH.⁴⁴ A

compound that has similar or better crystal inhibition that does not lead to alkalinization may be preferred in patients with a high urine pH. The analysis of molecules in Figure 1A shows that many polyprotic acids do not satisfy the fourth criterion. Exceptions are HCA and ICA. *In vitro* studies show that HCA is more potent than CA at low concentrations (ca. < 60 μ g/mL), while both molecules are equivalent inhibitors at high concentrations. Human trials also revealed that HCA is bioavailable with oral intake, ²⁸ confirming HCA satisfies at least two of the four criteria. In this study, bulk crystallization indicates that ICA is comparable to CA as an inhibitor of COM crystallization (Figure 4C). Information of ICA toxicity and bioavailability is unknown. Moreover, answers to criterion one (tolerability) have yet to be adequately addressed for HCA and ICA.

Here, we test the efficacy of citrate analogues as COM crystal growth inhibitors in a physiologically relevant medium: human urine. For these *in vitro* assays, we used eight urine samples from patients with kidney stones. The samples were chosen to have hypocitraturia out of concern that urine samples with high citrate might not be able to show a dose response to additional citrate as a crystal growth inhibitor. The citrate, calcium, and oxalate concentrations of the urine samples were 128 ± 36 , 122 ± 43 , and 18 ± 5 mg/L, respectively. A representative set of growth curves are presented in Figure 5A showing the temporal

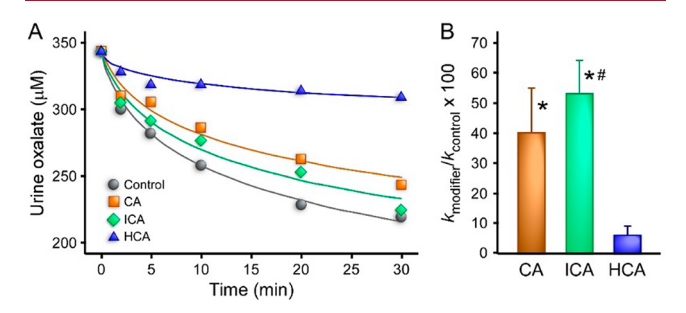


Figure 5. Calcium oxalate growth assay in human urine. (A) The reduction in urine oxalate concentration is monitored as a function of time using 2 mM inhibitor. The data presented are a representative study from a single urine sample. Lines are extrapolations to guide the eye. (B) Relative growth constants calculated in the presence of CA, ICA, and HCA from growth assays performed in eight urine samples. The average percent inhibition of calcium oxalate growth for HCA, CA, and ICA is $96 \pm 3\%$, $60 \pm 15\%$ and $47 \pm 11\%$, respectively. (*p = 0.01 vs HCA, #p = 0.05 vs CA). Urine samples were collected from stone-formers with relatively low citrate levels (ca. $C_{\rm CA} = 0.68$ mM).

depletion of oxalate during calcium oxalate crystallization. The results are quantified by calculating growth constants k_i (see Methods) and expressing the results as a ratio of the growth constant in the presence of the inhibitors to the growth constant of the urine sample without added inhibitors (Figure 5B). Our findings indicate that CA and ICA have comparable rates of inhibition, consistent with measurements made in simple salt solutions (Figure 1C). Interestingly, HCA is significantly more potent, resulting in ca. $96 \pm 3\%$ inhibition of calcium oxalate growth compared to a value of 60% measured in a salt solution.

Unexpectedly, the efficacy of HCA is higher in urine compared to its measured inhibitory effect in assays employing simplistic growth solutions (i.e., aqueous solutions of supersaturated calcium oxalate and 150 mM NaCl). Our findings seem to indicate a synergistic effect between HCA and urinary constituents that leads to an additional 36% inhibition—an

outcome that is not encountered for CA and ICA. In prior studies we have shown that a combination of CA and urinary constituents (e.g., chondroitin sulfate) can increase the percent inhibition of COM crystal growth by ca. 20%. For the *in vitro* assays presented in Figure 5, it is impossible for us to speculate on the nature of the synergistic interaction(s) and their resulting mode(s) of action on crystal growth inhibition given the fact that urine is a highly complex blend of species. Notably, urine contains ca, 3100 small molecule metabolites and over 1800 proteins. Nevertheless, our findings lend additional support for HCA as a putative therapeutic of calcium oxalate stone disease. Moreover, these studies highlight the benefit of using physiologically relevant media to assess the effect of molecular inhibitors on pathological crystallization.

CONCLUSION

In summary, we have shown that a majority of small polyprotic acids are ineffective inhibitors of COM crystallization. Conversely, acidic molecules decorated with alcohols have a more pronounced impact on COM growth. A detailed analysis of three citrate analogues revealed that subtle variations in alcohol placement lead to distinct binding modes that alter growth along orthogonal crystallographic directions. When evaluating inhibitor-crystal interactions, we posit that the criterion for strain-induced dissolution of COM crystal surfaces is best correlated to a vectorized displacement owing to the pulling of atoms/molecules outward from the crystal-solvent interface. In this study, we quantify the strain imposed by select modifiers using the net displacement δ of atoms within the crystal lattice as well as their net angle $\Delta\Phi$ of displacement. This is a relatively new phenomenon in which there remain many unanswered questions pertaining to the methods of predicting (and quantifying) the strain imposed by modifier binding to crystal surfaces, and discerning the experimental conditions that lead to strain-induced dissolution. This observation was made for hyroxycitrate where an unexpected outcome of this study was its enhanced efficacy in urine compared to laboratory measurements in simple salt solutions. Comparisons of polyprotic acids also identified isocitrate as a moderately effective inhibitor with comparable efficacy as citrate, but an unexpectedly distinct specificity for binding to COM crystal surfaces that differs from either of its molecular analogues. Given the potential problems of using the current drug for oxalate stone disease, citrate, in patients with a high urine pH and the number of patients who cannot tolerate potassium citrate, identification of potential replacements is a notable advancement toward the development of better preventative treatments for urolithiasis.

METHODS SECTION

Materials. The following reagents were purchased from Sigma-Aldrich (St. Louis, MO): calcium chloride dihydrate (99+%), sodium oxalate (>99%), oxalic acid (99%), malonic acid (99%), succinic acid (99%), glutaric acid (99%), adipic acid (99%), malic acid (%), tartaric acid (%), tricarballylic acid (99%), dimethyl hydroxyglutaric acid (98%); sodium citrate tribasic dihydrate (≥99.0%), DL-isocitric acid disodium hydrate (93%), potassium hydroxycitrate tribasic monohydrate (95%), butanetetracarboxylic acid (99%), sodium hydroxide (98%), and hydrochloric acid (37%). Methyl oxalic acid (97%) was purchased from AK Scientific Inc. and sodium chloride (99.9%) was purchased from JT Baker. Deionized (DI) water used in all experiments was prepared with an Aqua Solutions RODI-C-12A purification system (18.2 MΩ). All reagents were used as received without further purification.

Bulk Crystallization Assays. Calcium oxalate monohydrate (COM) crystallization was carried out using a reported protocol $^{24,28,30-32}$ in 20 mL glass vials. First, NaCl was dissolved in DI water followed by the addition of CaCl2 stock solution. The sample vial was then placed in an oven at 60 °C for 1 h to ensure the solution had reached the set temperature for crystallization. The vial was removed from the oven, Na2C2O4 stock solution was immediately added dropwise while the solution was continuously stirred at a rate of ca. 400 rpm, and the vial was returned to the oven. To investigate the effect of inhibitors on COM crystallization, a desired quantity of each polyprotic acid was added dropwise to the growth solution prior to Na₂C₂O₄ addition. The final growth solution had a composition of 0.7 mM CaCl₂: 0.7 mM Na₂C₂O₄: 150 mM NaCl: 60 µg/mL inhibitor and a total volume of ca. 10 mL. A clean glass slide (1.3 × 1.3 cm²) was placed at the bottom of the vial to collect crystals for microscopy studies. Crystallization was performed at 60 °C for 3 days without agitation. The glass slide (substrate) was removed from the solution and dried at room temperature prior to analysis. The pH of COM growth solution was set to ca. 6.2 by adding an appropriate quantity of sodium hydroxide and measuring the solution with an Orion 3-Star Plus pH benchtop meter and ROSS Ultra electrode (8102BNUWP).

The binding affinity of crystal growth inhibitors on COM surfaces was analyzed by comparing the morphology and dimensions of COM crystals prepared in the absence and presence of polyprotic acids. A Leica DM2500-M optical microscope was used to obtain brightfield images in reflectance mode to quantify the effect of inhibitors by comparing the aspect ratio (AR) of resulting COM crystals (note that AR is defined as the ratio of [001] and [010] dimensions). A minimum of 100 crystals from three separate batches were measured to obtain an average AR.

The effect of inhibitors on the kinetics of COM crystallization was measured using a calcium ion selective electrode (ISE) from ThermoScientific equipped with an Orion 9720BNWP ionplus electrode. ISE measurements track the temporal change of free calcium ion concentration in the growth solution during crystallization, which captures the effects of inhibitors on nucleation as well as crystal growth.³¹ Solutions were prepared similar to those of bulk crystallization with a final solution composition of 0.5 mM CaCl₂: 0.5 mM Na₂C₂O₄: 150 mM NaCl: 60 μg/mL inhibitor (supersaturation ratio S = 3.8 was calculated using solubility product 1.66×10^{-9} M²).⁴ ISE measurements were performed at room temperature with constant stirring at ca. 1200 rpm to minimize the induction period.^{24,31} The electrodes were calibrated using three known concentrations of standard calcium solution (0.1, 1.0, and 10.0 mM) diluted from 0.1 M stock solution (Orion Ion Plus). An ionic strength adjuster (ISA, Thermo Scientific) was added to the standard solutions in a 1:50 volume ratio of ISA-to-standard. Plots of consumed calcium ion concentration as a function of time were constructed for each experiment where the approximate linear region signifies the depletion of free calcium ions. Inhibitor efficacy was quantified by comparing the rate of calcium depletion in the absence and in the presence of each polyprotic acid. A minimum of six measurements were performed for each inhibitor.

Scanning Probe Microscopy. In situ atomic force microscopy (AFM) was performed using a Digital Instruments Multimode IV (Santa Barbara, CA) equipped with a fluid cell (model MTFML) to examine the effect of citrate analogues on COM surface growth in real time. COM crystals were anchored on a magnetic specimen disk (Ted Pella) using a thin layer of thermally curable epoxy (MasterBond EP21AOLV). COM crystals prepared on glass slides were transferred to the specimen disk by gently pressing the glass slides onto epoxy which was partially cured at 60 °C for ca. 20 min. The specimen disks were then placed in an oven at 60 °C for an additional 3 h to completely cure the epoxy. AFM measurements were performed in contact mode using silicon nitride probes with gold reflex coating and a spring constant of 0.15 N/m (Olympus, TR800PSA). In situ experiments were performed under supersaturated conditions (S = 4.1) to monitor the growth of COM {100} surfaces by tracking step advancement in the absence and in the presence of selected inhibitors. Growth solutions used for in situ AFM had a final composition of 0.18 mM CaCl₂: 0.18 mM Na₂C₂O₄: x

 μ g/mL inhibitor (where x = 0-0.45). In order to maintain a constant supersaturation ratio, the growth solutions were continuously delivered to the fluid cell via a designated inlet port with in-line mixing configuration⁴⁸ using a dual syringe pump (CHEMYX, Fusion 200) with a combined flow rate of 0.2 mL/min. Selected inhibitors were introduced to the growth solution by adding a desired quantity of polyprotic acid to the Na₂C₂O₄ solution. Images during *in situ* experiments were captured with a scan rate of 13.2 Hz at 256 lines/scan.

Density Functional Theory (DFT) Calculations. DFT calculations can provide accurate adsorption trends on materials and elucidate the thermodynamics of particle stabilization and/or growth as shown in relevant work on metal nanoparticle growth in the presence of ligands. 49-51 The DFT calculations were performed by applying the same methodology as reported in our previous work.²⁸ Briefly, we performed cluster-type DFT calculations using the Turbomole package. 52 We used the BP86 functional 53,54 with the def2-SV(P) basis set⁵⁵ and accounted for dispersion energy corrections (for capturing hydrogen bonding) through the D3 method.⁵⁶ The resolution of the identities (RI)⁵⁷ approximation along with multipole accelerated resolution of indices (MARI-J)⁵⁸ were used to accelerate the calculations. We accounted for solvent effects through the COSMO continuum solvation model (solvent = water, $\varepsilon = 78.46$). The COM particle with the (100) surface termination consisted of 168 atoms (Ca₂₄C₄₈O₉₆), whereas the one with the (021) termination consisted of 133 atoms ($Ca_{19}C_{38}O_{76}$). The (100) and (021) surfaces were kept frozen during inhibitor relaxations unless otherwise stated.

The binding energy (BE) of inhibitors and oxalate to crystal surfaces is defined as

$$BE = E_{\text{inhibitor} + COM} - E_{\text{inhibitor}} - E_{COM}$$
 (2)

where E_x represents the total electronic energy of species x. For calculations of the "inhibitor + COM" species, the deprotonated forms of the acids were placed on the COM surfaces and hydrogens were added far away from the interaction center and in antidiametric positions on the COM particle to neutralize the system. In the previous BE expression, the $E_{\rm inhibitor}$ corresponds to the total energy of the nondissociated acid. As a result, eq 1 can capture the adsorption strength trends of the deprotonated acids on the COM surface, while keeping our system consistently in a neutral charge state. Analogous to the previous expression, the BE of the complexes used in determining the affinity of HCA, CA, ICA, and Ox for Ca²⁺ is defined as

BE (complex) =
$$E_{\text{complex}} + n \frac{d}{2} E_{\text{H}_2} - n \frac{d}{2} E_{\text{Ca}} - n E_{\text{inhibitor}}$$
 (3)

where n represents the number of organic molecules in the complex, d is the deprotonation state of the inhibitor (i.e., d=1 corresponds to single, d=2 to double, and d=3 to triple deprotonated states, equivalently), and E_x represents the electronic energy of species x. The inhibitor is again in the nondissociated form in the solution phase and we use H_2 as a reference state for the hydrogens of the acids. To sample multiple modifier-surface conformations, approximately four different modifier conformations were relaxed on each surface for every BE calculation reported (with only the lowest values being reported). As further validation of the reported conformations as minima vibrational analysis verified the absence of any imaginary frequencies on the complexes or inhibitors interacting with COM crystal surfaces. We also performed calculations with both isomers of ICA (as experiments used racemic mixture) and found little difference in their binding to the (100) surface (see Figure S7).

For calculations where the surface of COM was allowed to relax, the oxalate molecules nearest the inhibitors in the first layer of atoms were allowed to relax. For the COM (100) surface, 16 atoms were relaxed, while for COM (021) 18 atoms were relaxed. The average displacement (δ) was calculated as

$$\delta = \left[\sum_{i=1}^{N_{\text{atoms}}} \left((x_{i,\text{frozen}} - x_{i,\text{relaxed}})^2 + (y_{i,\text{frozen}} - y_{i,\text{relaxed}})^2 + (z_{i,\text{frozen}} - z_{i,\text{relaxed}})^2 \right] / \left[N_{\text{atoms}} \right]$$

$$(4)$$

where $N_{\rm Atoms}$ is the number of atoms relaxed and x, y, and z represent the spatial coordinates of the atoms relaxed in both their initial and final states. To quantify the angle of the displacement observed in the surfaces due to the presence of the inhibitors we constructed a resultant displacement vector $(\hat{\delta})$ defined as

$$\hat{\delta} = \left[\sum_{i=1}^{N_{\text{atoms}}} (x_{i,\text{frozen}} - x_{i,\text{relaxed}}), \sum_{i=1}^{N_{\text{atoms}}} (y_{i,\text{frozen}} - y_{i,\text{relaxed}}) \right]$$

$$, \sum_{i=1}^{N_{\text{atoms}}} (z_{i,\text{frozen}} - z_{i,\text{relaxed}})$$
(5)

while the surface normal vector (SN) was defined from calcium atoms sitting in the plane of the surface. To calculate the angle of displacement we used:

$$\Phi = \cos^{-1}[(\hat{\delta} \cdot SN)/(|\hat{\delta}| * |SN|)]$$
(6)

This vectorized displacement is further illustrated in Figure S9.

COM Growth in Human Urine. Inhibition of COM crystal growth was measured with a seeded assay in urine from kidney stone patients. Urine from patients with kidney stones was obtained from discarded samples from a clinical laboratory (Western IRB protocol #20162248). Urine samples were selected to have a citrate concentration of less than 200 mg/L to be used in the study. All samples were brought to pH 6.0 using HCl or NaOH as needed. Samples were centrifuged at 3000 rpm for 15 min to remove particulate matter. After centrifugation, four 5.6 mL aliquots of the urine were introduced into 15 mL polystyrene tubes that were placed in an incubator at 37 °C with constant stirring. Stock solutions of citrate, hydroxycitrate and isocitrate (all obtained from Sigma-Aldrich, St Louis MO) were prepared with 30 mM concentration and brought to pH 6.0. To three of the tubes of urine, 0.4 mL of each inhibitor was added for a final volume of 6 mL per tube and an incremental increase in concentration of 2 mM for the inhibitors. In a fourth tube of urine, 0.4 mL of water was added to act as a control.

A COM seed crystal slurry was made using 25 mg of COM crystals in 10 mL of distilled water. The slurry was magnetically stirred overnight prior to use. Urine oxalate was measured at baseline (time = 0) and 300 μ L of the crystal slurry was pipetted into each tube of urine to initiate the growth assay. A fraction of urine (750 μ L) was removed at the following time-points: 2, 5, 10, 20, 30, and 60 min. The urine samples were centrifuged through a 10 kd filter to remove crystals (Nanosep, Pall Corporation, Port Washington NY). The filtrate was then acidified with HCl and urine oxalate was measured enzymatically using oxalate oxidase (Trinity Biotech; Wicklow, Ireland).

The growth constants were calculated using the method of Meyer and Smith.⁶⁰ The oxalate concentration from 60 min in the control sample was used as the saturation concentration of oxalate for that particular urine. Concentrations of calcium, oxalate, and other solutes varied among urine samples; therefore, each experiment required that the growth constants for the inhibitors be expressed in relation to the control for that same experiment.

ASSOCIATED CONTENT

Supporting Information

The Supporting Information is available free of charge on the ACS Publications website at DOI: 10.1021/acs.cgd.8b00945.

Additional figures summarizing the results of bulk crystallization in the presence and absence of ICA; step velocity data from AFM measurements of COM (100) growth in the presence of ICA; AFM images of COM

(010) surface growth in the presence of ICA; DFT simulations of acid binding to free calcium and select COM crystal surfaces; DFT calculations of the binding energy between acids and COM crystal surfaces. Additional tables listing the dissociation constants of acids in Figure 1A; surface relaxation vectorization data from DFT calculations (PDF)

AUTHOR INFORMATION

Corresponding Author

*E-mail: jrimer@central.uh.edu.

ORCID ®

Giannis Mpourmpakis: 0000-0002-3063-0607 Jeffrey D. Rimer: 0000-0002-2296-3428

Author Contributions

J.C. performed AFM measurements, SEM crystal characterization, and ISE bulk crystallization assays; M.G.T. performed DFT calculations; I.G. performed the crystallization assays in urine; J.D.R., G.M., and J.R.A. designed the experiments; J.D.R. wrote the paper with help from G.M. and J.R.A.; all authors discussed the results and commented on the manuscript.

Notes

The authors wish to note that J.D.R. and J.R.A. have filed patent applications on the use of inhibitors as crystal growth inhibitors of pathological calcification, and J.D.R. has filed a similar patent for inhibitors of L-cystine crystallization.

The authors declare no competing financial interest.

ACKNOWLEDGMENTS

J.D.R. acknowledges support from the National Science Foundation (1207441) and the Welch Foundation (E-1794). G.M. acknowledges support by the National Science Foundation (CBET-CAREER program) under Grant No. 1652694 and by the University of Pittsburgh seed funding. M.G.T. acknowledges support by the National Science Foundation Graduate Research Fellowship under Grant No. 1247842. Computational support was provided by the Center for Research Computing at the University of Pittsburgh, and the Extreme Science and Engineering Discovery Environment, which is supported by the NSF (ACI-1053575).

REFERENCES

- (1) Weissbuch, I.; Leiserowitz, L. Interplay between malaria, crystalline hemozoin formation, and antimalarial drug action and design. *Chem. Rev.* **2008**, *108*, 4899–4914.
- (2) Fiddis, R. W.; Vlachos, N.; Calvert, P. D. Studies of urate crystallization in relation to gout. *Ann. Rheum. Dis.* **1983**, 42, 12–15.
- (3) Dorozhkin, S. V. Calcium orthophosphates. J. Mater. Sci. 2007, 42, 1061–1095.
- (4) Holan, K. R.; Holzbach, R. T.; Hermann, R. E.; Cooperman, A. M.; Claffey, W. J. Nucleation time- Key factor in the pathogenesis of cholesterol gallstone disease. *Gastroenterology* **1979**, *77*, 611–617.
- (5) Bushinsky, D. A. Nephrolithiasis. J. Am. Soc. Nephrol. 1998, 9,
- (6) De Yoreo, J. J.; Vekilov, P.G. Principles of crystal nucleation and growth. In *Biomineralization*; Dove, P. M.; De Yoreo, J. J.; Weiner, S., Eds.; Mineralogical Society: Washington, D.C., 2003; pp 57–93.
- (7) Dove, P.; De Yoreo, J.Inhibition of CaCO₃ crystallization by small molecules: the magnesium example. In *Nanoscale Structure and Assembly at Solid-Fluid Interfaces*; Liu, X., De Yoreo, J., Eds.; Kluwer Academic Publishers, 2004.

(8) Dey, A.; de With, G.; Sommerdijk, N. In situ techniques in biomimetic mineralization studies of calcium carbonate. *Chem. Soc. Rev.* **2010**, *39*, *397*–409.

- (9) Meldrum, F. C. Calcium carbonate in biomineralisation and biomimetic chemistry. *Int. Mater. Rev.* **2003**, 48, 187–224.
- (10) Meldrum, F. C.; Colfen, H. Controlling Mineral Morphologies and Structures in Biological and Synthetic Systems. *Chem. Rev.* **2008**, 108, 4332–4432.
- (11) Evans, J. S. "Tuning in" to mollusk shell nacre- and prismatic-associated protein terminal sequences. Implications for biomineralization and the construction of high performance inorganic-organic composites. *Chem. Rev.* **2008**, *108*, 4455–4462.
- (12) Falini, G.; Albeck, S.; Weiner, S.; Addadi, L. Control of aragonite or calcite polymorphism by mollusk shell macromolecules. *Science* **1996**, 271, 67–69.
- (13) Young, J. R.; Didymus, J. M.; Bown, P. R.; Prins, B.; Mann, S. Crystal assembly and phylogenetic evolution in heterococcoliths. *Nature* **1992**, *356*, 516–518.
- (14) Dunlop, J. W. C.; Fratzl, P. Biological composites. *Annu. Rev. Mater. Res.* **2010**, *40*, 1–24.
- (15) Coe, F. L.; Parks, J. H.; Asplin, J. R. Medical progress The pathogenesis and threatment of kidney stones. *N. Engl. J. Med.* **1992**, 327, 1141–1152.
- (16) Nancollas, G. H.; Gardner, G. L. Kinetics of crystal-growth of calcium-oxalate monohydrate. *J. Cryst. Growth* **1974**, 21, 267–276.
- (17) Wesson, J. A.; Ward, M. D. Pathological biomineralization of kidney stones. *Elements* **2007**, *3*, 415–421.
- (18) Kittanamongkolchai, W.; Vaughan, L. E.; Enders, F. T.; Dhondup, T.; Mehta, R. A.; Krambeck, A. E.; McCollough, C. H.; Vrtiska, T. J.; Lieske, J. C.; Rule, A. D. The Changing Incidence and Presentation of Urinary Stones Over 3 Decades. *Mayo Clin. Proc.* **2018**, 93, 291–299.
- (19) Addadi, L.; Weiner, S. Interactions between acidic proteins and crystals- Stereochemical requirements in biomineralization. *Proc. Natl. Acad. Sci. U. S. A.* **1985**, 82, 4110–4114.
- (20) Fleming, D. E.; van Bronswijk, W.; Ryall, R. L. A comparative study of the adsorption of amino acids on to calcium minerals found in renal calculi. *Clin. Sci.* **2001**, *101*, 159–168.
- (21) Taller, A.; Grohe, B.; Rogers, K. A.; Goldberg, H. A.; Hunter, G. K. Specific adsorption of osteopontin and synthetic polypeptides to calcium oxalate monohydrate crystals. *Biophys. J.* **2007**, *93*, 1768–1777.
- (22) Wang, L. J.; Zhang, W.; Qiu, S. R.; Zachowicz, W. J.; Guan, X. Y.; Tang, R. K.; Hoyer, J. R.; De Yoreo, J. J.; Nancollas, G. H. Inhibition of calcium oxalate monohydrate crystallization by the combination of citrate and osteopontin. *J. Cryst. Growth* **2006**, *291*, 160–165.
- (23) Asplin, J. R.; Arsenault, D.; Parks, J. H.; Coe, F. L.; Hoyer, J. R. Contribution of human uropontin to inhibition of calcium oxalate crystallization. *Kidney Int.* **1998**, *53*, 194–199.
- (24) Farmanesh, S.; Ramamoorthy, S.; Chung, J.; Asplin, J. R.; Karande, P.; Rimer, J. D. Specificity of growth inhibitors and their cooperative effects in calcium oxalate monohydrate crystallization. *J. Am. Chem. Soc.* **2014**, *136*, 367–376.
- (25) Atmani, F.; Khan, S. R. Role of urinary bikunin in the inhibition of calcium oxalate crystallization. *J. Am. Soc. Nephrol.* **1999**, *10*, S385—S388
- (26) Wesson, J. A.; Worcester, E. M.; Wiessner, J. H.; Mandel, N. S.; Kleinman, J. G. Control of calcium oxalate crystal structure and cell adherence by urinary macromolecules. *Kidney Int.* **1998**, *53*, 952–957.
- (27) Guo, S. W.; Ward, M. D.; Wesson, J. A. Direct visualization of calcium oxalate monohydrate crystallization and dissolution with atomic force microscopy and the role of polymeric additives. *Langmuir* **2002**, *18*, 4284–4291.
- (28) Chung, J. H.; Granja, I.; Taylor, M. G.; Mpourmpakis, G.; Asplin, J. R.; Rimer, J. D. Molecular modifiers reveal a mechanism of pathological crystal growth inhibition. *Nature* **2016**, 536, 446.
- (29) Li, M.; Zhang, J.; Wang, L.; Wang, B.; Putnis, C. V. Mechanisms of modulation of calcium phosphate pathological mineralization by mobile and immobile small-molecule inhibitors. *J. Phys. Chem. B* **2018**, 122, 1580–1587.

(30) Farmanesh, S.; Alamani, B. G.; Rimer, J. D. Identifying alkali metal inhibitors of crystal growth: a selection criterion based on ion pair hydration energy. *Chem. Commun.* **2015**, *51*, 13964–13967.

- (31) Farmanesh, S.; Chung, J.; Chandra, D.; Sosa, R. D.; Karande, P.; Rimer, J. D. High-throughput platform for design and screening of peptides as inhibitors of calcium oxalate monohydrate crystallization. *J. Cryst. Growth* **2013**, 373, 13–19.
- (32) Farmanesh, S.; Chung, J.; Sosa, R. D.; Kwak, J. H.; Karande, P.; Rimer, J. D. Natural promoters of calcium oxalate monohydrate crystallization. *J. Am. Chem. Soc.* **2014**, *136*, 12648–12657.
- (33) Rimer, J. D.; An, Z. H.; Zhu, Z. N.; Lee, M. H.; Goldfarb, D. S.; Wesson, J. A.; Ward, M. D. Crystal growth inhibitors for the prevention of L-cystine kidney stones through molecular design. *Science* **2010**, 330, 337–341.
- (34) Chung, J.; Sosa, R.; Rimer, J. D. Elucidating the Effects of Polyprotic Acid Speciation in Calcium Oxalate Crystallization. *Cryst. Growth Des.* **2017**, *17*, 4280–4288.
- (35) Shirane, Y.; Kagawa, S. Scanning electron microscopic study of the effect of citrate and pyrophosphate on calcium oxalate crystal morphology. *J. Urol.* **1993**, *150*, 1980–1983.
- (36) Qiu, S. R.; Wierzbicki, A.; Orme, C. A.; Cody, A. M.; Hoyer, J. R.; Nancollas, G. H.; Zepeda, S.; Yoreo, J.J. De Molecular modulation of calcium oxalate crystallization by osteopontin and citrate. *Proc. Natl. Acad. Sci. U.S.A.* 2004, 101, 1811–1815.
- (37) Weaver, M. L.; Qiu, S. R.; Hoyer, J. R.; Casey, W. H.; Nancollas, G. H.; Yoreo, J.J. De Improved model for inhibition of pathological mineralization based on citrate-calcium oxalate monohydrate interaction. *ChemPhysChem* **2006**, *7*, 2081–2084.
- (38) Cabrera, N.; Vermileya, D. A., The growth of crystals form solution. In *Growth and Perfection of Crystals*; Doremus, R. H., Roberts, B. W.; Turnbul, D., Eds.; Wiley: New York, 1958; pp 393–410.
- (39) Bliznakov, G. Sur le mechanisme de l'action des additifs adsorbants dans la croissance cristalline. In *Adsorption et Croissance Cristalline*; Centre National de la Recherche Scientifique: Paris, 1965; pp 291–300.
- (40) Lovette, M. A.; Browning, A. R.; Griffin, D. W.; Sizemore, J. P.; Snyder, R. C.; Doherty, M. F. Crystal shape engineering. *Ind. Eng. Chem. Res.* **2008**, *47*, 9812–9833.
- (41) Snyder, R. C.; Doherty, M. F. Predicting crystal growth by spiral motion. *Proc. R. Soc. London, Ser. A* **2009**, *465*, 1145–1171.
- (42) Winn, D.; Doherty, M. F. Modeling crystal shapes of organic materials grown from solution. *AIChE J.* **2000**, *46*, 1348–1367.
- (43) Sizemore, J. P.; Doherty, M. F. A new model for the effect of molecular imposters on the shape of faceted molecular crystals. *Cryst. Growth Des.* **2009**, *9*, 2637–2645.
- (44) Hamm, L. L. Renal handling of citrate. *Kidney Int.* **1990**, *38*, 728–735.
- (45) Bouatra, S., Aziat, F.; Mandal, R.; Guo, A.C.; Wilson, M. R.; Knox, C.; Bjorndahl, T. C.; Krishnamurthy, R.; Saleem, F.; Liu, P.; Dame, Z. T.; Poelzer, J.; Huynh, J.; Yallou, F. S.; Psychogios, N.; Dong, E.; Bogumil, R.; Roehring, C.; Wishart, D. S. The Human Urine Metabolome. *Plos One*, 2013. 8.
- (46) Marimuthu, A.; O'Meally, R. N.; Chaerkady, R.; Subbannayya, Y.; Nanjappa, V.; Kumar, P.; Kelkar, D. S.; Pinto, S. M.; Sharma, R.; Renuse, S.; Goel, R.; Christopher, R.; Delanghe, B.; Cole, R. N.; Harsha, H. C.; Pandey, A. A Comprehensive Map of the Human Urinary Proteome. *J. Proteome Res.* **2011**, *10*, 2734–2743.
- (47) Tomazic, B. B.; Nancollas, G. H. A study of the phase-transformation of calcium oxalate trihydrate-monohydrate. *Invest. Urol.* **1979**, *16*, 329–335.
- (48) Jung, T.; Sheng, X. X.; Choi, C. K.; Kim, W. S.; Wesson, J. A.; Ward, M. D. Probing crystallization of calcium oxalate monohydrate and the role of macromolecule additives with in situ atomic force microscopy. *Langmuir* **2004**, *20*, 8587–8596.
- (49) Li, Q., Luo, T. Y.; Taylor, M. G.; Wang, S. X.; Zhu, X. F.; Song, Y. B.; Mpourmpakis, G.; Rosi, N. L.; Jin, R. C.Molecular "surgery" on a 23-gold-atom nanoparticle. *Sci. Adv.*, 2017. 3.
- (50) Mpourmpakis, G.; Vlachos, D. G. Growth Mechanisms of Metal Nanoparticles via First Principles. *Phys. Rev. Lett.*, **2009**. *102*.

(51) Taylor, M. G.; Mpourmpakis, G. Thermodynamic stability of ligand-protected metal nanoclusters. *Nat. Commun.*, 2017. 8.

- (52) Åhlrichs, R.; Bar, M.; Haser, M.; Horn, H.; Kolmel, C. Electronic-structure calculations on workstation computers- The program system turbomole. *Chem. Phys. Lett.* **1989**, *162*, 165–169.
- (53) Becke, A. D. Density-functional exchange-energy approximation with correct asymptotic behavior. *Phys. Rev. A: At., Mol., Opt. Phys.* **1988**, 38, 3098–3100.
- (54) Perdew, J. P. Density-functional approximation for the correlation energy of the inhomogeneous electron gas. *Phys. Rev. B: Condens. Matter Mater. Phys.* **1986**, 33, 8822–8824.
- (55) Weigend, F.; Haser, M.; Patzelt, H.; Ahlrichs, R. RI-MP2: optimized auxiliary basis sets and demonstration of efficiency. *Chem. Phys. Lett.* **1998**, 294, 143–152.
- (56) Grimme, S., Antony, J.; Ehrlich, S.; Krieg, H. A consistent and accurate ab initio parametrization of density functional dispersion correction (DFT-D) for the 94 elements H-Pu. *J. Chem. Phys.*, **2010**, 132.
- (57) Feyereisen, M.; Fitzgerald, G.; Komornicki, A. Use of approximate integrals in ab initio theory- An application in MP2 enegry calculations. *Chem. Phys. Lett.* **1993**, 208, 359–363.
- (58) Weigend, F.; Haser, M. RI-MP2: first derivatives and global consistency. *Theor. Chem. Acc.* **1997**, 97, 331–340.
- (59) Klamt, A.; Schuurmann, G. COSMO- A new approach to dielectric screening in solvents with explicit expressions for the screening energy and its gradient. *J. Chem. Soc., Perkin Trans.* 2 **1993**, 799–805.
- (60) Hida, H.; Yamada, T.; Yamada, Y. Absolute configuration of hydroxycitric acid produced by microorganisms. *Biosci., Biotechnol., Biochem.* **2006**, 70, 1972–1974.